WARWICK
THE UNIVERSITY OF WARWICK

Original citation:
Perry, David, Momotenko, Dmitry, Lazenby, Robert A., Kang, Minkyung and Unwin, Patrick R.. (2016) Characterization of nanopipettes. Analytical Chemistry.

Permanent WRAP URL:
http://wrap.warwick.ac.uk/79023

Copyright and reuse:
The Warwick Research Archive Portal (WRAP) makes this work by researchers of the University of Warwick available open access under the following conditions. Copyright © and all moral rights to the version of the paper presented here belong to the individual author(s) and/or other copyright owners. To the extent reasonable and practicable the material made available in WRAP has been checked for eligibility before being made available.

Copies of full items can be used for personal research or study, educational, or not-for profit purposes without prior permission or charge. Provided that the authors, title and full bibliographic details are credited, a hyperlink and/or URL is given for the original metadata page and the content is not changed in any way.

Publisher's statement:
"This document is the Accepted Manuscript version of a Published Work that appeared in final form in Analytical Chemistry, copyright © American Chemical Society after peer review and technical editing by the publisher.
To access the final edited and published work
http://pubs.acs.org/page/policy/articlesonrequest/index.html ."

A note on versions:
The version presented here may differ from the published version or, version of record, if you wish to cite this item you are advised to consult the publisher's version. Please see the 'permanent WRAP url' above for details on accessing the published version and note that access may require a subscription.

For more information, please contact the WRAP Team at: wrap@warwick.ac.uk

warwick.ac.uk/lib-publications

Characterization of Nanopipettes

David Perry,[1,2] Dmitry Momotenko,[1] Robert A. Lazenby,[1] Minkyung Kang[1] and Patrick R. Unwin[1,*]

[1]Department of Chemistry, [2]MOAC Doctoral Training Centre, University of Warwick, Coventry, CV4 7AL, United Kingdom

***Corresponding Author**

p.r.unwin@warwick.ac.uk

ABSTRACT

Nanopipettes are widely used in electrochemical and analytical techniques as tools for sizing, sequencing, sensing, delivery and imaging. For all of these applications, the response of a nanopipette is strongly affected by its geometry and surface chemistry. As the size of nanopipettes becomes smaller, precise geometric characterization is increasingly important, especially if nanopipette probes are to be used for quantitative studies and analysis. This contribution highlights the combination of data from voltage-scanning ion conductivity experiments, transmission electron microscopy (TEM) and finite element method (FEM) simulations to fully characterize nanopipette geometry and surface charge characteristics, with an accuracy not achievable using existing approaches. Indeed, it is shown that presently used methods for nanopipette characterization can lead to highly erroneous information on nanopipettes. The new approach to characterization further facilitates high-level quantification of the behavior of nanopipettes in electrochemical systems, as demonstrated herein for a scanning ion conductance microscope (SICM) setup.

INTRODUCTION

Nanopipettes are becoming increasingly important tools across nanoscience for their functional versatility and ease of fabrication.[1] Typically fabricated from glass (*e.g.* borosilicate) or quartz capillaries, nanopipettes are produced through the application of heat whilst a pulling force is applied to each end of the capillary. By adjusting the pulling parameters, the probe geometry can be finely tuned and it is possible to produce probes with opening diameters as low as tens of nanometers.[2, 3] While the simplest nanopipettes contain just a single channel, multichannel devices are also possible, which increases the versatility of nanopipettes for nanoscience applications.[4, 5] The channels can be open[5, 6] (filled with electrolyte and a control electrode) or functionalized with deposited carbon, for example, to produce ultramicroelectrodes (UMEs)[7, 8] that can also be further functionalized[9-11] to tune the sensory properties. Nanoelectrodes can also be fabricated by electrochemically plating nanopipettes with a variety of different metals.[12]

Applications of nanopipettes include as tools for sizing, counting,[13-17] and sequencing of single particles or molecules.[18-20] These applications use the changes in ionic current through the end of the nanopipette (with an applied bias), as a single entity passes through the end of the probe, to provide diagnostic information. Furthermore, these probes constitute powerful tools for the delivery of molecules, including drugs and other stimuli,[16, 21, 22] to surfaces and interfaces. Nanopipettes have also been used extensively as chemical sensors, detecting, for example, pH,[9] sodium,[23] potassium[24] and other ions as well as dopamine[25] and DNA molecules.[16, 18, 26] Recently, the capability of using functionalized nanopipettes for single molecule electrochemical detection has been revealed.[27] Beyond electroanalysis, nanopipettes are finding novel applications as devices for electrospray mass-spectrometry.[28, 29]

Nanopipette probes, employed in different types of scanning probe microscopy (SPM) techniques,[5, 11, 30] are used increasingly for the study of interfacial properties across a

range of materials including electrodes and living cells.[3, 31, 32] Examples of SPM techniques that can employ nanopipettes include scanning electrochemical microscopy (SECM),[30, 33] scanning ion conductance microscopy (SICM),[31, 34-38] SICM-SECM[9, 39] and scanning electrochemical cell microscopy (SECCM).[5, 40] Beyond the surface or interface being investigated, the size, shape and surface properties of the nanopipette may also strongly influence the SPM response, such that robust theoretical models, underpinned by a complete knowledge of the nanopipette characteristics, are needed for quantitative analysis.

This work concerns the procedure for the characterization of nanopipettes filled with electrolyte solution, which is the main configuration for the wide range of applications above. Although the focus is on single barreled nanopipettes, and their use in bulk solution and SICM, the approach described could be extended to multi-barreled nanopipettes[4, 10] and other SPM configurations.[5, 9] For SPM applications, it is important to know the geometry of a nanopipette, specifically the aperture size, the inner pipette half cone angle and the thickness of the glass, because this plays a significant role in the probe response. In particular, the size of the nanopipette opening typically determines the image resolution (estimated to be about $3r_o$ where r_o is the radius of the pipette opening),[35, 41] whilst the thickness of the nanopipette walls at the opening can affect how the nanopipette responds upon approach to interfaces of different topographies.[35, 42] Herein, we utilize transmission electron microscopy (TEM) to obtain the nanopipette geometry with high precision and complementary finite element method (FEM) simulations allow us to match ionic current signals under an applied bias with theory. This provides information on the mass transport characteristics with high accuracy. Experimental measurements and FEM simulations further allow the characterization of nanopipette surface charge, which is integral to quantitative surface charge mapping using SICM,[43-46] and is expected to be important in sizing applications.[47, 48]

MATERIALS AND METHODS

Nanopipette probes

Nanopipettes were pulled from either quartz capillaries (o.d. 1 mm, i.d. 0.5 mm, Friedrich & Dimmock, pulling parameters: Line 1: Heat 750, Fil 4, Vel 30, Del 150, Pul 80, Line 2: Heat 650, Fil 3, Vel 40, Del 135, Pul 150) or borosilicate glass capillaries (o.d. 1.2 mm, i.d. 0.69 mm, Harvard Apparatus, pulling parameters: Line 1: Heat 330, Fil 3, Vel 30, Del 220, Pul -, Line 2: Heat 330, Fil 3, Vel 40, Del 180, Pul 120) using a laser puller (P-2000, Sutter Instruments. Dimensions of the individual nanopipettes used in experiments in this work were measured after experiments through a combination of TEM and optical microscopy. Typically, quartz nanopipettes presented an aperture diameter of 30-60 nm whilst borosilicate nanopipettes had a diameter of 150-200 nm (measured accurately).

Solutions

Milli-Q reagent grade water (resistivity ca. 18.2 MΩ cm at 25°C) was used for all solutions. 1 mM, 10 mM and 500 mM KNO_3 (Sigma-Aldrich) solutions were prepared and used for the SICM cyclic voltammetry (CV) experiments. KNO_3 was used as a typical 1:1 electrolyte, although in principle any electrolyte could be used for these studies.

Instrumentation

The instrumentation used has been described elsewhere.[38, 43, 44] The current-to-voltage converter used to measure currents was custom built. Data recording, as well as the probe position and voltage output control, was performed using a custom written LabVIEW (2013, National Instruments) program through an FPGA card. The SICM probe movement normal to the substrate was controlled using a piezoelectric positioning stage with a travel range of 38 μm (P-753-3CD, Physik Instrumente). A lock-in amplifier (SR830, Stanford Research Systems) was used to apply the oscillating bias in the BM-SICM setup and to extract the AC ion current amplitude and phase used for surface charge mapping and SICM feedback.

Nanopipette voltammetry

Nanopipettes were bathed in, and filled with, the aqueous solution of interest, and one Ag/AgCl QRCE was inserted into the nanopipette and another similar electrode was placed in bulk solution. This electrode maintains a stable potential in a wide range of aqueous media, including KNO_3, because although AgCl is only sparingly soluble, its dissolution kinetics are fast,[49] so that the wire is bathed in saturated AgCl solution. The potential applied to the QRCE in the nanopipette was swept between -0.4 V and 0.4 V, with respect to the bulk QRCE, at a rate of 50 mV/s and the current recorded at the QRCE in bulk solution.

Optical Microscopy

Optical images were taken of the nanopipette taper and were analyzed using Adobe Illustrator (CC 2015) to provide estimates of the inner and outer diameter at lengths 20 μm to 300 μm from the nanopipette tip for use in FEM simulations.

TEM Imaging of Nanopipettes

Before TEM imaging, solution was removed from a nanopipette that had been used for current-voltage (*I-V*) measurements, and the nanopipette was then placed in a deionized water bath overnight to remove as much remaining salt residue from the end of the nanopipette as possible before being left to dry for 1 day. A JEOL 2000FX microscope operating at 200 kV accelerating voltage, equipped with a GATAN ORIUS 11 megapixel digital camera, was used for TEM tip characterization. Adobe Illustrator CC 2015 graphics software was used to obtain nanopipette dimensions with pixel level (<1 nm at the highest magnification) precision.

FEM Simulations of Nanopipettes in Bulk Solution

A two-dimensional axisymmetric FEM model was constructed to calculate the *I-V* characteristics of a nanopipette in bulk solution of high (500 mM) and low (10 mM or 1 mM)

ionic strength. Simulations were constructed in Comsol Multiphysics (version 4.4), using the transport of diluted species and electrostatics modules. Dimensions of the nanopipettes at various distances up the pipette, from the opening, were obtained from TEM and optical images. This ensured that the geometry of nanopipettes was reproduced faithfully in the simulations. Data for the nanopipettes, whose *I-V* characteristics are discussed in this work, are given in Supporting Information, Table S1.

The simulation was as outlined previously,[43] with details given in Supporting Information, section SI-1. A bulk domain of 160 μm × 160 μm was implemented and a nanopipette length of 300 μm was used at which point the nanopipette inner diameter was in all cases larger than 10 μm and so the resistance contribution from the remainder of the nanopipette would be minimal. A surface charge was included on the lowest 20 μm of the nanopipette where the mesh size was also smallest (maximum 0.5 nm). The bias between the bulk of the nanopipette with respect to the solution bulk was changed between 0.4 V and -0.4 V as in the experimental CVs reported below and the current extracted, in order to generate *I-V* curves. For simulations performed in 10 mM and 1 mM, the surface charge applied to the nanopipette was adjusted (as the only variable) until matching with experimental data to give a value for the pipette surface charge.

BM-SICM Surface Charge Mapping of Glass Substrate

Surface charge mapping was performed as described in previous work.[43, 45] A quartz nanopipette was translated towards a glass substrate (glass bottomed Petri dish with detachable coverslip, WillcoWells), with no net bias applied between the 2 QRCEs, rather just a small harmonic oscillation of the bias (270 Hz, 28 mV rms amplitude about 0 V). Upon detection of the surface through a 0.5° increase in the recorded AC phase (see below for method of distance determination), probe translation stopped automatically and a CV was performed from 0 V to 0.4 V to -0.4 V and back to 0 V, for surface charge detection, at a rate of 0.2 V/s. The nanopipette was then retracted 500 nm (~10 tip radii) and the same CV

profile performed in bulk for characterization of the nanopipette probe surface charge. For the tips used herein, 500 nm corresponded to be around 10 tip diameters and was sufficiently far away from the surface to represent the bulk SICM response, which is typically seen around 1 tip diameter away from the substrate.[36] No observable difference was seen between CVs performed at greater separation distances than this.

Quantification of Surface Charge

For quantification of substrate surface charge, the surface charge of the nanopipette was obtained in the same way as above using the analysis of the bulk CV. A working distance for the near-surface experimental measurement was obtained by first calculating the system differential capacitance at no net applied bias according to:[50]

$$C = \frac{\tan\theta}{2\pi fR} \quad (1)$$

where θ is the AC phase signal recorded experimentally, *f* is the AC oscillation frequency and *R* is the system resistance around 0 V, obtainable from an *I-V* curve in bulk solution. A circuit diagram representing the components of the BM-SICM setup is presented in Supporting Information, Figure S4. A FEM simulated approach curve was then calculated at a range of tip-substrate separations to obtain the distance-dependent system resistance. We could then use equation 1 to calculate θ at each separation distance, because simulations showed that the capacitance did not change with distance (i.e. is dominated by the nanopipette itself). The resulting working curve of θ against tip-substrate separation allowed the evaluation of the separation at which the surface measurement was made. Once the working distance was known, the surface charge of the substrate was varied in the simulation until the simulated *I-V* curve matched that obtained experimentally, with the smallest residual error. Care should be taken in this approach, ensuring that the nanopipette is aligned perpendicular to the sample of interest, as a slope of the sample could affect the working distance and hence surface charge values obtained. If the slope of the sample was

known or minimal over the dimensions of the nanopipette opening, the effects could be modeled or would be negligible. [42]

RESULTS AND DISCUSSION

Evaluation of Existing Methods For Nanopipette Characterization

Scanning electron microscopy (SEM) of nanopipette openings has commonly been used to extract an estimate for the aperture radius and the glass thickness at the opening.[3, 26, 29, 51] However, for nanopipettes that have openings less than 50 nm in diameter, the resolution of SEM is insufficient. The characterization of nanopipettes using SEM also becomes more difficult at this scale as it requires the nanopipette to be sputtered with a conducting metal, which affects the nanopipette dimensions. SEM has other limitations as a tool for characterizing nanopipettes of this size, as it provides little information about the nanopipette lumen size beyond at the opening. The nanopipette resistance properties are dependent on the nanopipette inner angle and how the lumen size varies with distance into the nanopipette. Full characterization of nanopipettes requires that these dimensions are obtained.

Hitherto, two approaches are commonly taken in order to characterize nanopipettes in the absence of more direct tools. Method 1 assumes that the ratio between the outer and inner diameter of a nanopipette remains constant to that at the nanopipette opening,[13, 41, 52] and, as such, the inner nanopipette angle can be calculated by using the relationship:

$$\tan a_{inner} = \frac{\tan a_{outer}}{r_{OI}} \quad (2)$$

where α_{outer} is the outer nanopipette angle, estimated from SEM images and r_{OI} is the ratio between the outer and inner pipette radii at the nanopipette opening.

Method 2 involves approximating the nanopipette as a truncated hollow cone[13, 31, 41, 53-57] in order to model its resistive properties. The resistance then depends on the inner cone angle and aperture radius according to:[53, 54]

$$R_p = \frac{1}{\kappa \pi r_i \tan\beta} + R_{access} \approx \frac{1}{\kappa \pi r_i \tan\beta} + \frac{1}{4\kappa r_i} \quad (3)$$

or equivalent equations, where R_p is the nanopipette resistance, r_i the inner pipette radius, κ is the solution conductivity and β is the inner nanopipette half cone angle. Using such equations, the resistive properties can be estimated given knowledge of the nanopipette radius and cone angle estimate, or the nanopipette radius can be back-calculated from experimental resistance values and some input value for the inner cone angle. These approaches are widely used[31, 52-54, 56] but require an estimate for the nanopipette inner angle, which cannot be obtained directly near the nanopipette opening using SEM, and to date has usually been estimated from the outer pipette angle obtained in SEM images.[55, 57-59] Evidently, this approach fails if the assumption about a constant inner angle does not hold. Method 1 and 2 will both be examined below to evaluate their suitability in nanopipette characterization and modeling, and compared to the method that we develop herein.

The surface charge density of a nanopipette also strongly influences the resulting *I-V* characteristics.[22, 60-63] Glass and quartz both exhibit negatively charged surface charge under typical experimental conditions (neutral pH, aqueous solutions) owing to the presence of silanol groups that dissociate (pK_a 7.5).[64] Ion current rectification phenomena (ICR) are manifest when the Debye length is even a small fraction of the dimension of the nanopipette opening,[60] resulting in a diminished ionic current with positive tip bias applied and an enhanced current when the polarity is reversed, compared to expectations if the nanopipette were uncharged.[43, 45, 60, 62]

Analytical approaches, such as utilizing equation 3 or similar equations for calculating the nanopipette radius or resistive properties, often at a fixed applied bias,[55, 56]

may evidently become inaccurate under these conditions, as the surface charge of the nanopipette is not generally considered. While there has been much work on the study and simulation of the ICR phenomena at nanopipettes in low ionic strength,[60, 62, 63] quantification of the nanopipette surface charge and understanding the nanopipette current response is a difficult task owing to a lack of more complete tip characterization methods.

Recently it has been shown that TEM offers an attractive means for visualizing nanopipettes.[65, 66] Here, we show that by combining TEM and optical microscopy of nanopipettes with data from ion conductance experiments, it is possible to obtain the most precise representation of the nanopipette geometry and properties, which provides a platform for a wide range of quantitative applications.

Characterization of Nanopipettes in High Ionic Strength Media

Example TEM images of one of each of the quartz and borosilicate nanopipettes characterized in this work by *I-V* measurements are shown in Figure 1a and 1b, respectively. A full example sequence of TEM images of a quartz nanopipette at each magnification utilized is provided in Supporting Information, Figure S2. These nanopipettes did not exhibit a purely conical geometry and the inner angle of the nanopipettes used in this work was seen to change significantly (2 —12°) up the length of the nanopipette taper as shown in Figure 1c, with the greatest change in the 500 nm nearest to the nanopipette opening. Further data are given in Table S1 in Supporting Information.

Typical SICM experiments are performed in moderate [19] to high ionic strengths (>100 mM),[3, 31, 32, 45, 67, 68] as are many nanopipette measurements.[14, 15, 18, 19] Under these conditions, the diffuse double layer is expected to be compressed to a sub-nanometer scale, and therefore undetectable, level according to:[50]

$$\frac{1}{k} = \left(\frac{\varepsilon \varepsilon_0 k_B T}{2 n^0 z^2 e^2} \right)^{0.5} \qquad (4)$$

for a *z*:*z* electrolyte where $1/\kappa$ is the Debye length, ε and ε_0 are the dielectric constants of the bulk material and vacuum, respectively, T is the temperature, k_B is the Boltzmann constant, z is the charge of the monovalent electrolyte ion and n^0 is the number concentration of each ion in the solution.

The voltammetric characteristics for two nanopipettes, Tip 1 and Tip 2, are presented in Figure 2 and both exhibit almost ideal ohmic response with minimal nanopipette charge effects on the ionic current, as would be expected under these conditions.[60] Employing a nanopipette geometry with dimensions extracted from TEM data, in the simulation gives excellent agreement to experimental data (red lines) for both of the nanopipettes, with no adjustable parameters. Note that for the simulations, concentration dependent diffusion coefficients were used, calculated from:[69]

$$D_i = D_i^{\infty}[1 + C_i(\frac{\partial \ln g_i}{\partial C_i})] \quad (5)$$

where D_i^{∞} is the infinitely dilute diffusion coefficient of species *i*, C_i is its concentration and γ_i its activity coefficient. For KNO_3 at an ionic strength of 500 mM this yielded diffusion coefficients of 1.45×10^{-5} cm^2/s and 1.41×10^{-5} cm^2/s for K^+ and NO_3^- respectively. Whilst the approaches outlined here have been demonstrated for single-barreled nanopipettes, the principles could naturally be extended for the consideration of dual or multi-barreled nanopipettes. By performing TEM imaging of a nanopipette from different angles, accurate dimensions could be obtained regardless of whether the nanopipette exhibited axial symmetry and this could be incorporated into a 3D FEM model for quantitative analysis of voltammetric properties.

Having shown that TEM characterization of nanopipettes results in excellent agreement between experiment and simulated conductivity data, Method 1 and Method 2 are now evaluated using Tip 1 as an example. Firstly in Method 1, if the assumption was

made that the ratio of the inner to outer dimensions of the nanopipette remained constant up the nanopipette taper length, as is commonly done,[13,31, 52, 70] the result is a significant underestimation of the nanopipettes resistive properties. A FEM simulation was performed using the varying outer angle of the nanopipette up its length, which might be reasonably obtained from SEM data, to estimate the inner angle and hence dimensions, according to equation 2, keeping r_{oi} constant as calculated at the nanopipette opening (r_{oi} =1.47 for Tip 1 from TEM data). From the resulting *I-V* curve depicted in Figure 3a, it can be seen that the match to the experimental data is now rather poor (contrasting with Figure 2a where TEM data were used). This more simplistic analysis to estimate the inner geometry of the nanopipette greatly underestimates the inner tip dimensions and hence the resistance properties of the nanopipette by around 50% at the extreme potentials of the *I-V* curve. This error could be even greater if a constant outer (and hence inner angle) was assumed, as is sometimes done in this field.

Next, Method 2 is considered which, as mentioned above, assumes a conical nanopipette geometry, and is often utilized to model the nanopipette resistance properties, or deduce the nanopipette radius.[31, 52-54, 56] Such an approach is very sensitive to the inner half cone angle chosen (equation 3). It has already been seen that the angle can change along the length of the nanopipette (Figure 1c) and will vary depending on the pulling parameters used for nanopipette fabrication. Quoted values for inner half cone angles range greatly, from $1.5° - 13°$ for different nanopipettes,[52, 55, 58, 71] and it has even been estimated to vary by as much as 2.5° between the same type of nanopipette.[59] However, it is important to point out that in all of these cases the estimate was not obtained using a suitable technique, as discussed above.

The black line in Figure 3b shows the effect of varying inner half cone angle on the predicted ionic current in 500 mM KNO_3 according to equation 3 at a tip bias of 0.4 V, assuming the nanopipette radius to be that obtained for Tip 1 from TEM data (R_i = 25 nm). It

can be seen that even small variations of the inner angle result in a large change in the nanopipette current response. The red line in Figure 3b utilizes the observed *I-V* characteristics of Tip 1 to consider how the choice of inner half cone angle would affect the prediction for the nanopipette opening size, according to equation 3, again with R_i = 25 nm. It can be seen that even a small variation of the inner cone angle assumed has a significant impact on the resulting nanopipette radius estimate.

Tip 1 has a measured radius of 25 nm, at the very end, and with this knowledge Method 2, yields an inner half cone angle of 3.7°, which should be compared with the actual profile in Figure 1c.

Quantifying Nanopipette Surface Charge in Low Ionic Strength

The charge on nanopipettes can also have a major impact on applications in sizing,[47] delivery and detection[18, 26] as well as imaging.[43, 45, 46] Furthermore, when deployed in SICM, nanopipettes are very promising for surface charge mapping. [43, 44] If the resistance is used to estimate the conical dimensions (equation 3) of a nanopipette, it is important to point out that such an approach is likely to fail in low ionic strength media, where the Debye length is longer, according to equation 4, especially if single potential measurements are made, which do not reveal surface charge effects. The *I-V* characteristics for quartz nanopipettes that were filled and bathed in 10 mM (Tip 3, Figure 4a) and 1 mM (Tip 5, Figure 4b) KNO_3 solutions exhibited an ICR response, which manifests more strongly at 1 mM, resulting in a greater rectification ratio, the ratio between the currents at the positive and negative extreme potential limits of the *I-V* curve.[60, 61] ICR was also seen at borosilicate glass nanopipettes, as in Figure 4c, in 10 mM KNO_3. More examples for each of these conditions are presented in Supporting Information, Figure S3. These characteristics, where the current is smaller at positive tip bias than at negative tip bias indicate that the nanopipette is negatively charged.[61]

Because the nanopipette geometry is known with high accuracy from TEM, the

surface charge on the nanopipette is the only adjustable parameter in FEM simulations to match to *I-V* experiments under these conditions. For the quartz nanopipettes used in this work, the surface charge was between -14 mC/m^2 and -16 mC/m^2 (at pH 6.2), a narrow range of values where the simulated *I-V* curves closely matched the experimental voltammograms (Figure 4). The noise level in these voltammetric experiments was 3 pA (peak-to-peak), which was much smaller than the difference between the currents at the extreme potentials of the simulated CVs (-0.4 V) with different surface charges depicted in Figure 4, (e.g. approximately 10 pA in the case of Figure 4a and b). This highlights the accuracy with which the surface charge could be determined (i.e. to better than 1 mC/m^2).

Importantly, there was no significant difference between the surface charges obtained in 10 mM (Figure 4a) and 1 mM KNO_3 (Figure 4b) solutions, giving confidence in this result. For the borosilicate glass nanopipettes studied, experimental and simulated *I-V* curves, presented in Figure 4c indicate a pipette wall surface charge of between -30 mC/m^2 and -40 mC/m^2. This higher charge on the borosilicate glass explains why it is possible to observe the effects of ICR, even with relatively large nanopipette sizes.[60-62]

There is much debate about the charge on glass nanopipettes and glass substrates, owing to a lack of techniques to robustly probe the surface charge of extended substrates. Consequently, a wide range of values have been quoted for the surface charge from -0.0001 mC/m^2 – -240 mC/m^2.[46] Some, but not all, of this variation in the surface charge of glass can be due to the fact that these measurements are made at a range of pH values.[64] The characterization methods advocated herein provide a means of unambiguously quantifying the surface charge of typical nanopipettes.

Quantifiable Surface Charge Mapping of Extended Substrates

The more precise nanopipette probe characterization method is particularly beneficial for SICM studies. To this end, single barreled quartz nanopipettes were approached to a glass substrate in a BM-SICM scheme, as described previously.[43] Upon detecting the surface

through an increase in the AC phase of 0.5° (corresponding to a distance of 10 ± 3 nm, see Figure 5a and Supporting Information, Figure S5), a CV measurement was performed with the net bias between the two QRCEs varied from 0 V, the approach bias, to +0.4 V to -0.4 V and back to 0 V. It has been demonstrated previously that the BM-SICM technique is insensitive to substrate surface charge and the phase or current amplitude only depends on distance when no net bias is applied.[43] ICR was seen at the quartz nanopipette in bulk solution (diminished current at positive tip bias compared to negative tip bias), which was magnified when the tip was near the surface. This can be seen in Figure 5b for Tip 4 whose surface charge was determined in bulk to be -16 mC/m^2 (Supporting Information, Figure S3a).

A FEM simulation was performed, with the nanopipette at the determined working distance (10 nm). The surface charge density applied to the substrate in the simulation was then varied (as the only adjustable parameter), yielding surface *I-V* curves presented in Figure 5c. The best fit was obtained with a surface charge density of around -30 mC/m^2, similar to the borosilicate glass nanopipettes.

CONCLUSIONS

It has been demonstrated that visualization of nanopipettes by TEM and optical microscopy, in combination with data for *I-V* measurements and FEM simulations, provides an holistic view of the geometry, properties and response of nanopipettes under electrochemical bias. Simulations of ion transport at high ionic strength, with the nanopipette geometry obtained precisely from TEM micrographs, results in strong agreement between simulated *I-V* curves and experimental data that can be trusted owing to no other assumptions being made about the nanopipette geometry or electrolyte properties, i.e. there are no adjustable parameters in the modelling. It is particularly important to note that in this work we have shown that the probe can easily be characterized by TEM after a set of *I-V* measurements or SICM

experiments, and the inner dimensions of the nanopipette can be obtained with high accuracy.

The new approach we propose contrasts with methods used hitherto, which rely on the use of analytical equations to model *I-V* curves with a highly idealized geometry. In these methods, the nanopipette opening that is obtained is strongly dependent on the choice of inner angle chosen to represent the nanopipette geometry. Our paper shows that nanopipettes do not necessarily have a conical shape and also that the outer and inner angles are very different, and vary with height along the nanopipette.

Through the use of FEM simulations it also becomes possible to further characterize nanopipettes in terms of their surface charge, as exemplified in our work for both quartz and borosilicate nanopipettes, for which robust values over small ranges have been obtained. Finally, by characterizing the nanopipette geometry and surface charge fully, it then becomes possible to quantify the surface charge of extended substrates in an SICM format, enhancing the SICM technique and its capability for functional mapping.

CONFLICT OF INTEREST

The authors declare no competing financial interest.

ACKNOWLEDGEMENT

This work was supported by the European Research Council through Project ERC-2009 AdG 247143-QUANTIF (R.A.L. and M.K.), the EPSRC through the MOAC DTC, grant number EP/F500378/1 (D.P.) and a Marie Curie IntraEuropean Fellowship 626158 FUNICIS (D.M.).

Supporting Information Available: The SI includes the FEM model equations and boundary conditions, a series of TEM images at the different magnifications utilized in this work, a table of dimensions obtained for each characterized nanopipette as well as more surface charge estimates for nanopipettes in bulk solution. A circuit representation of the BM-SICM

setup to aid the understanding of equation 1 and a simulated approach AC approach curve is also included.

REFERENCES

1. Morris, C. A.; Friedman, A. K.; Baker, L. A. Analyst 2010, 135, 2190-2202.
2. Takahashi, Y.; Murakami, Y.; Nagamine, K.; Shiku, H.; Aoyagi, S.; Yasukawa, T.; Kanzaki, M.; Matsue, T. Phys. Chem. Chem. Phys. 2010, 12, 10012-10017.
3. Shevchuk, A. I.; Frolenkov, G. I.; Sánchez, D.; James, P. S.; Freedman, N.; Lab, M. J.; Jones, R.; Klenerman, D.; Korchev, Y. E. Angew. Chem. Int. Ed. 2006, 118, 2270-2274.
4. Paulose Nadappuram, B.; McKelvey, K.; Byers, J. C.; Güell, A. G.; Colburn, A. W.; Lazenby, R. A.; Unwin, P. R. Anal. Chem. 2015.
5. Ebejer, N.; Güell, A. G.; Lai, S. C. S.; McKelvey, K.; Snowden, M. E.; Unwin, P. R. Annu. Rev. Anal. Chem. 2013, 6, 329-351.
6. Li, Q.; Xie, S.; Liang, Z.; Meng, X.; Liu, S.; Girault, H. H.; Shao, Y. Angew. Chem. Int. Ed. 2009, 48, 8010-8013.
7. Schrlau, M. G.; Dun, N. J.; Bau, H. H. ACS Nano 2009, 3, 563-568.
8. Takahashi, Y.; Shevchuk, A. I.; Novak, P.; Zhang, Y.; Ebejer, N.; Macpherson, J. V.; Unwin, P. R.; Pollard, A. J.; Roy, D.; Clifford, C. A.*, et al.* Angew. Chem. Int. Ed. 2011, 50, 9638-9642.
9. Nadappuram, B. P.; McKelvey, K.; Al Botros, R.; Colburn, A. W.; Unwin, P. R. Anal. Chem. 2013, 85, 8070-8074.
10. Takahashi, Y.; Shevchuk, A. I.; Novak, P.; Murakami, Y.; Shiku, H.; Korchev, Y. E.; Matsue, T. J. Am. Chem. Soc. 2010, 132, 10118-10126.
11. O'Connell, M. A.; Wain, A. J. Anal. Chem. 2014, 86, 12100-12107.
12. Hao, R.; Zhang, B. Anal. Chem. 2015, 88, 614-620.
13. Terejánszky, P.; Makra, I.; Fürjes, P.; Gyurcsányi, R. E. Anal. Chem. 2014, 86, 4688-4697.
14. Wang, Y.; Kececi, K.; Mirkin, M. V.; Mani, V.; Sardesai, N.; Rusling, J. F. Chem. Sci. 2013, 4, 655-663.
15. Edwards, M. A.; German, S. R.; Dick, J. E.; Bard, A. J.; White, H. S. ACS Nano 2015, 9, 12274-12282.
16. Ivanov, A. P.; Actis, P.; Jönsson, P.; Klenerman, D.; Korchev, Y.; Edel, J. B. ACS Nano 2015, 9, 3587-3595.
17. Liu, Y.; Yobas, L. Biosensors and Bioelectronics 2013, 50, 78-83.
18. Steinbock, L. J.; Otto, O.; Chimerel, C.; Gornall, J.; Keyser, U. F. Nano Lett. 2010, 10, 2493-2497.
19. Gong, X.; Patil, A. V.; Ivanov, A. P.; Kong, Q.; Gibb, T.; Dogan, F.; deMello, A. J.; Edel, J. B. Anal. Chem. 2014, 86, 835-841.
20. Fu, Y.; Tokuhisa, H.; Baker, L. A. Chemical Communications 2009, 4877-4879.
21. Babakinejad, B.; Jönsson, P.; López Córdoba, A.; Actis, P.; Novak, P.; Takahashi, Y.; Shevchuk, A.; Anand, U.; Anand, P.; Drews, A. Anal. Chem. 2013, 85, 9333-9342.
22. Shi, W.; Sa, N.; Thakar, R.; Baker, L. A. Analyst 2015, 140, 4835-4842.
23. Piper, J. D.; Clarke, R. W.; Korchev, Y. E.; Ying, L.; Klenerman, D. J. Am. Chem. Soc. 2006, 128, 16462-16463.

24. Takami, T.; Iwata, F.; Yamazaki, K.; Son, J. W.; Lee, J.-K.; Park, B. H.; Kawai, T. J. Appl. Phys. 2012, 111, 044702.
25. Rees, H. R.; Anderson, S. E.; Privman, E.; Bau, H. H.; Venton, B. J. Anal. Chem. 2015, 87, 3849-3855.
26. Karhanek, M.; Kemp, J. T.; Pourmand, N.; Davis, R. W.; Webb, C. D. Nano Lett. 2005, 5, 403-407.
27. Byers, J. C.; Paulose Nadappuram, B.; Perry, D.; McKelvey, K.; Colburn, A. W.; Unwin, P. R. Anal. Chem. 2015, 87, 10450-10456.
28. Yuill, E. M.; Sa, N.; Ray, S. J.; Hieftje, G. M.; Baker, L. A. Anal. Chem. 2013, 85, 8498-8502.
29. Yuill, E. M.; Shi, W.; Poehlman, J.; Baker, L. A. Anal. Chem. 2015.
30. Schulte, A.; Nebel, M.; Schuhmann, W. Annu. Rev. Anal. Chem. 2010, 3, 299-318.
31. Korchev, Y.; Milovanovic, M.; Bashford, C.; Bennett, D.; Sviderskaya, E.; Vodyanoy, I.; Lab, M. J. Microsc. 1997, 188, 17-23.
32. Shevchuk, A. I.; Gorelik, J.; Harding, S. E.; Lab, M. J.; Klenerman, D.; Korchev, Y. E. Biophys. J. 2001, 81, 1759-1764.
33. Amemiya, S.; Bard, A. J.; Fan, F.-R. F.; Mirkin, M. V.; Unwin, P. R. Annu. Rev. Anal. Chem. 2008, 1, 95-131.
34. Hansma, P.; Drake, B.; Marti, O.; Gould, S.; Prater, C. Science 1989, 243, 641-643.
35. Edwards, M. A.; Williams, C. G.; Whitworth, A. L.; Unwin, P. R. Anal. Chem. 2009, 81, 4482-4492.
36. Chen, C. C.; Zhou, Y.; Baker, L. A. Annu. Rev. Anal. Chem. 2012, 5, 207-28.
37. Happel, P.; Thatenhorst, D.; Dietzel, I. D. Sensors 2012, 12, 14983.
38. McKelvey, K.; Perry, D.; Byers, J. C.; Colburn, A. W.; Unwin, P. R. Anal. Chem. 2014, 86, 3639-46.
39. Morris, C. A.; Chen, C.-C.; Baker, L. A. Analyst 2012, 137, 2933-2938.
40. Ebejer, N.; Schnippering, M.; Colburn, A. W.; Edwards, M. A.; Unwin, P. R. Anal. Chem. 2010, 82, 9141-9145.
41. Rheinlaender, J.; Schäffer, T. E. J. Appl. Phys. 2009, 105, 094905.
42. Thatenhorst, D.; Rheinlaender, J.; Schäffer, T. E.; Dietzel, I. D.; Happel, P. Anal. Chem. 2014, 86, 9838-9845.
43. Perry, D.; Al Botros, R.; Momotenko, D.; Kinnear, S. L.; Unwin, P. R. ACS Nano 2015, 9, 7266-76.
44. McKelvey, K.; Kinnear, S. L.; Perry, D.; Momotenko, D.; Unwin, P. R. J. Am. Chem. Soc. 2014, 136, 13735-13744.
45. Perry, D.; Paulose Nadappuram, B.; Momotenko, D.; Voyias, P. D.; Page, A.; Tripathi, G.; Frenguelli, B. G.; Unwin, P. R. J. Am. Chem. Soc. 2016.
46. Sa, N.; Lan, W.-J.; Shi, W.; Baker, L. A. ACS Nano 2013, 7, 11272-11282.
47. Lan, W.-J.; Kubeil, C.; Xiong, J.-W.; Bund, A.; White, H. S. J. Phys. Chem. C 2014, 118, 2726-2734.
48. Henriquez, R. R.; Ito, T.; Sun, L.; Crooks, R. M. Analyst 2004, 129, 478-482.
49. Macpherson, J. V.; Unwin, P. R. J. Phys. Chem. 1995, 99, 14824-14831.
50. Bard, A. J.; Faulkner, L. R. Electrochemical Methods: Fundamentals and Applications; Wiley New York, 1980; Vol. 2.
51. Rheinlaender, J.; Schäffer, T. E. Soft Matter 2013, 9, 3230-3236.
52. Takahashi, Y.; Ito, K.; Wang, X.; Matsumae, Y.; Komaki, H.; Kumatani, A.; Ino, K.; Shiku, H.; Matsue, T. Electrochemistry 2014, 82, 331-334.

53. Actis, P.; Mak, A. C.; Pourmand, N. Bioanal. Rev. 2010, 1, 177-185.
54. Del Linz, S.; Willman, E.; Caldwell, M.; Klenerman, D.; Fernández, A.; Moss, G. Anal. Chem. 2014, 86, 2353-2360.
55. Ying, L.; White, S. S.; Bruckbauer, A.; Meadows, L.; Korchev, Y. E.; Klenerman, D. Biophys. J. 2004, 86, 1018-1027.
56. Caldwell, M.; Del Linz, S. J.; Smart, T. G.; Moss, G. W. Anal. Chem. 2012, 84, 8980-8984.
57. Sánchez, D.; Johnson, N.; Li, C.; Novak, P.; Rheinlaender, J.; Zhang, Y.; Anand, U.; Anand, P.; Gorelik, J.; Frolenkov, G. I. Biophys. J. 2008, 95, 3017-3027.
58. Chen, C.-C.; Derylo, M. A.; Baker, L. A. Anal. Chem. 2009, 81, 4742-4751.
59. Chen, C.-C.; Baker, L. A. Analyst 2011, 136, 90-97.
60. Wei, C.; Bard, A. J.; Feldberg, S. W. Anal. Chem. 1997, 69, 4627-4633.
61. White, H. S.; Bund, A. Langmuir 2008, 24, 2212-2218.
62. Momotenko, D.; Cortes-Salazar, F.; Josserand, J.; Liu, S.; Shao, Y.; Girault, H. H. Phys. Chem. Chem. Phys. 2011, 13, 5430-5440.
63. Kubeil, C.; Bund, A. J. Phys. Chem. C 2011, 115, 7866-7873.
64. Behrens, S. H.; Grier, D. G. J. Chem. Phys 2001, 115, 6716-6721.
65. Zhou, L.; Zhou, Y.; Baker, L. A. Electrochem. Soc. Interface 2014, 47.
66. Cai, H.; Wang, Y.; Yu, Y.; Mirkin, M. V.; Bhakta, S.; Bishop, G. W.; Joshi, A. A.; Rusling, J. F. Anal. Chem. 2015, 87, 6403-6410.
67. Klenerman, D.; Korchev, Y. E.; Davis, S. J. Curr. Opin. Chem. Biol. 2011, 15, 696-703.
68. Gorelik, J.; Shevchuk, A. I.; Frolenkov, G. I.; Diakonov, I. A.; Kros, C. J.; Richardson, G. P.; Vodyanoy, I.; Edwards, C. R.; Klenerman, D.; Korchev, Y. E. Proc. Natl. Acad. Sci. U. S. A. 2003, 100, 5819-5822.
69. Girault, H. H. Analytical and Physical Electrochemistry; CRC Press, 2004.
70. Rodgers, P. J.; Amemiya, S.; Wang, Y.; Mirkin, M. V. Anal. Chem. 2009, 82, 84-90.
71. Clarke, R. W.; Zhukov, A.; Richards, O.; Johnson, N.; Ostanin, V.; Klenerman, D. J. Am. Chem. Soc. 2013, 135, 322-9.

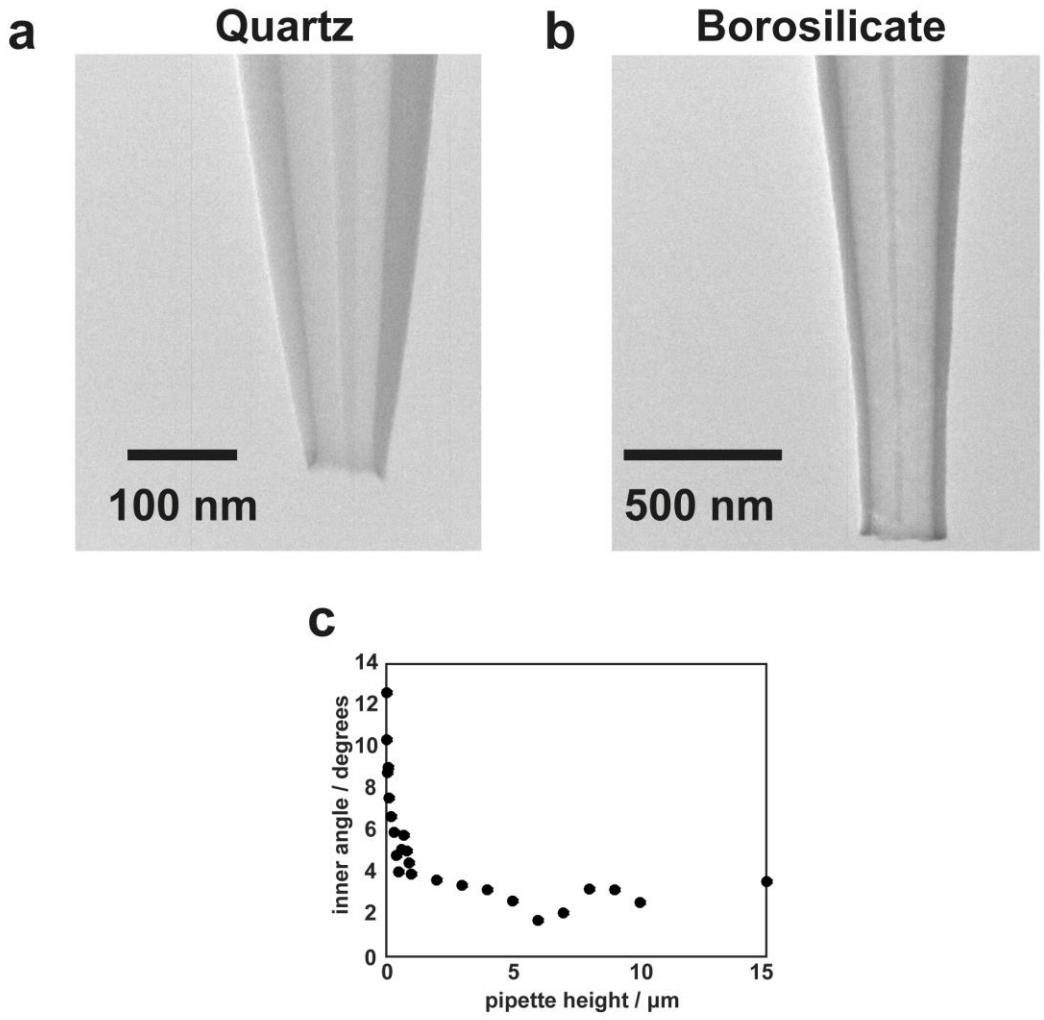

Figure 1: Typical TEM micrographs of quartz (**a**) and borosilicate (**b**) nanopipettes characterized after CV experiments had been performed. Dimensions were extracted from images with pixel (nm) level precision. The filament of the nanopipette, which aids their filling, can be seen down the centre of the TEM images, but has a negligible effect on the voltammetric characteristics. **c)** Plot of how the inner angle of Tip 1 varies up the length of the nanopipette. These data allow FEM models to faithfully reproduce the nanopipettes for ion conductance studies.

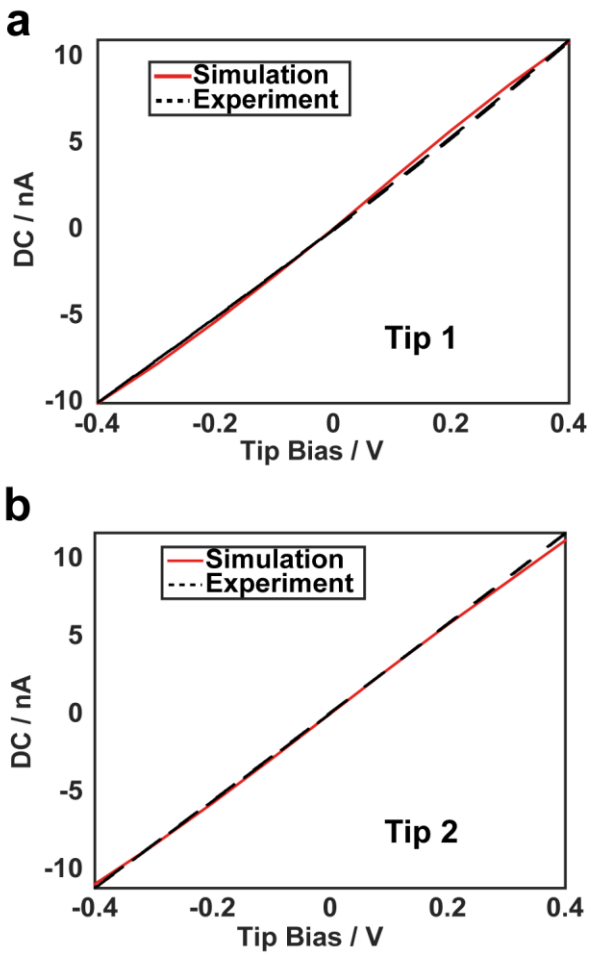

Figure 2: The *I-V* characteristics of Tip 1 (**a**) and Tip 2 (**b**) in high electrolyte conditions (500 mM KNO_3). An ohmic ion current-voltage response is seen and there is strong agreement between experiment (black) and the simulated response (red) based on the nanopipette dimensions extracted using TEM, with no adjustable parameters.

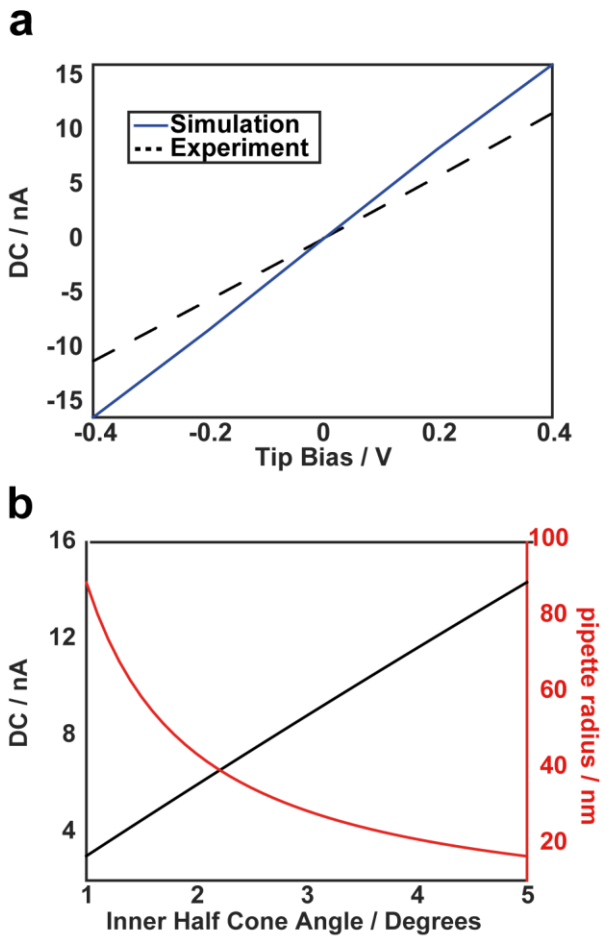

Figure 3 a) Simulation (blue), assuming that the ratio, r_{oi}, of the outer to inner wall thickness for Tip 1 remains the same as at the nanopipette opening (r_{oi} = 1.47), calculating inner dimensions relative to the measured outer dimensions from TEM (which could be obtainable using SEM) alongside the experimental data from Figure 2a. **(b)** FEM calculation of the ionic current at 0.4 V tip bias as a function of the inner half cone angle for the measured pipette radius for Tip 1 (25 nm) from TEM (black), together with calculated nanopipette radius as a function of inner half cone angle using the experimental resistance calculated from Figure 2a (red).

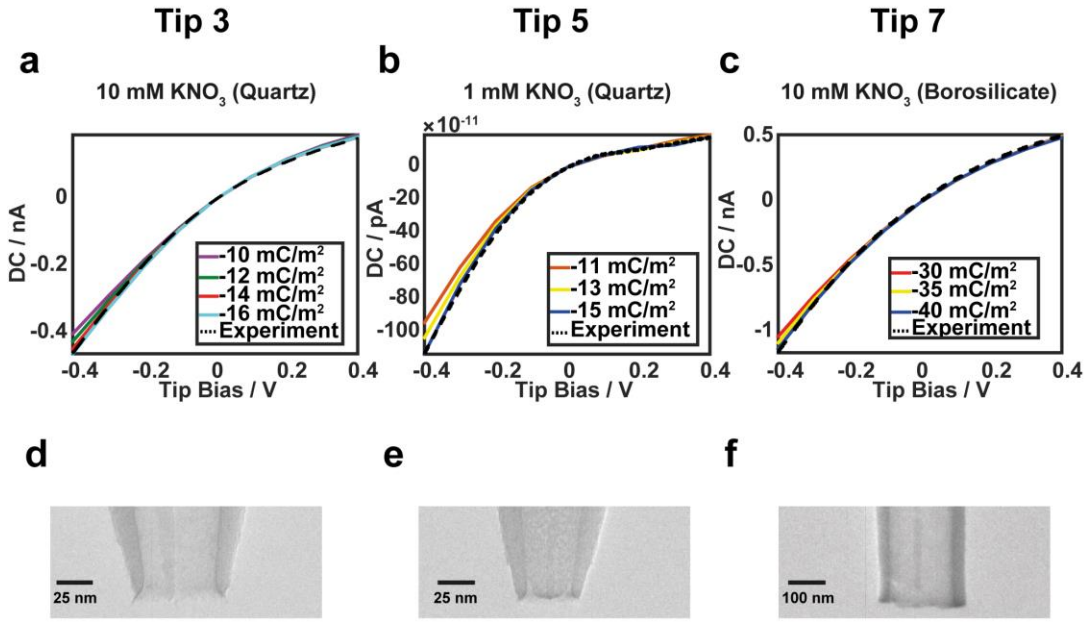

Figure 4: *I-V* characteristics of quartz nanopipettes at low ionic strength reveal ion current rectification in 10 mM KNO_3 (**a**), which is seen more strongly as the ionic strength decreases further to 1 mM KNO_3 (**b**). Larger borosilicate nanopipettes also exhibit ion current rectification and a correspondingly larger nanopipette surface charge is required to match the experimental response. The noise level for these experiments was 3 pA (peak-to-peak). Corresponding TEM images for each tip are shown (**d**-**f**). Note that the surface charge on the nanopipette is the only variable in the simulation to fit to the experimental data. The simulation results for different charges are shown as the colored lines.

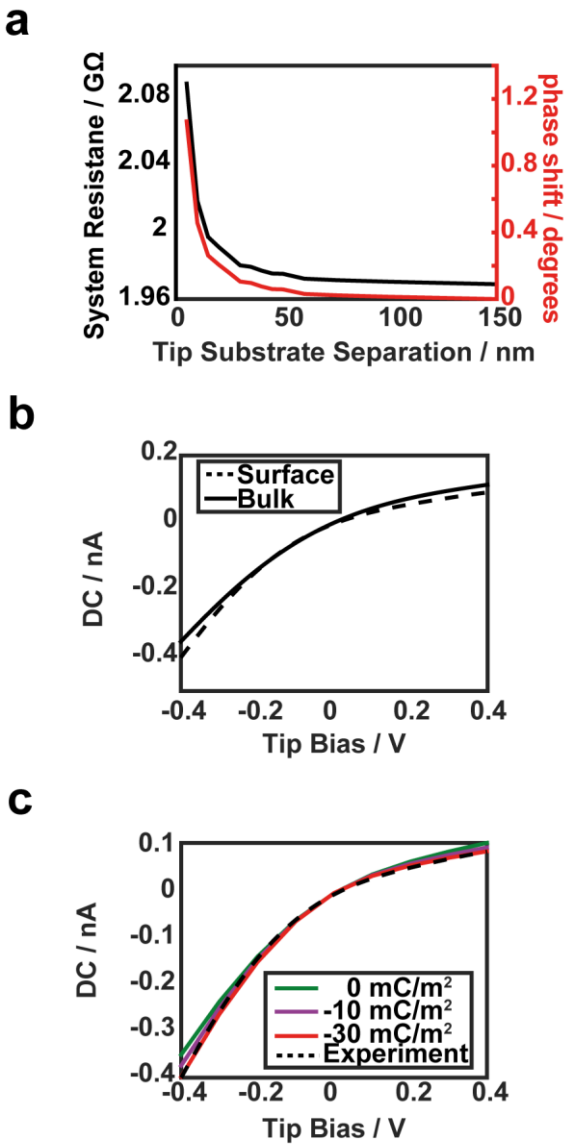

Figure 5. a) FEM simulations allow calculation of the system resistance for Tip 4 (black) as a function of tip-substrate separation at 0 V net bias from which the phase shift, as a function of distance, can be calculated (red), which can be used to estimate the working distance for surface charge experiments. **b)** *I-V* curves of Tip 4 in bulk solution and near (10 nm) from a glass surface in 10 mM KNO_3. **c)** Fits to the near-surface *I-V* curve with the charge on the substrate the only variable and the tip charge fixed at -16 mC/m^2 as measured in bulk solution (Supporting Information, Figure S3a).